KSOE

Journal of Ocean Engineering and Technology 37(4), 158-163, August, 2023
https://doi.org/10.26748/KSOE.2023.023

pISSN 1225-0767
eISSN 2287-6715

Original Research Article

Location Tracking of Drifting Container by Solitary Wave Load Using a Motion Analysis Program

Taegeon Hwang[1], Jiwon Kim[2], Dong-Ha Lee[3] and Jae-Cheol Lee[4]

[1]*Graduate Student, Department of Ocean Civil Engineering, Gyeongsang National University, Tongyeong, Korea*
[2]*Senior Engineer, Offshore Infrastructure Team, Harbor Department, Yooshin Engineering Corporation, Seoul, Korea*
[3]*Associate Professor, Department of Integrated Energy and Infra System, Kangwon National University, Chuncheon, Korea*
[4]*Graduate Student, Department of Integrated Energy and Infra System, Kangwon National University, Chuncheon, Korea*

KEYWORDS: Location tracking, Drifting objects, Drifting behavior, DIPP-Motion analysis, Solitary waves, Tsunamis

ABSTRACT: *Objects adrift can cause considerable damage to coastal infrastructure and property during tsunami and storm surge events. Despite the potential for harm, the drifting behavior of these objects remains poorly understood, thereby hindering effective prediction and mitigation of collision damage. To address this gap, this study employed a motion analysis program to track a drifting container's location using images from an existing laboratory experiment. The container's trajectory and velocity were calculated based on the positions of five markers strategically placed at its four corners and center. Our findings indicate that the container's maximum drift velocity and distance are directly influenced by the scale of the solitary wave and inversely related to the container's weight. Specifically, heavier containers are less likely to be displaced by solitary waves, while larger waves can damage coastal structures more. This study offers new insights into container drift behavior induced by solitary waves, with implications for enhancing coastal infrastructure design and devising mitigation strategies to minimize the risk of collision damage.*

1. Introduction

A tsunami is a phenomenon triggered by the displacement of the seafloor or the release of energy from an undersea earthquake or volcanic eruption. This event leads to alterations in water levels that propagate over great distances, eventually impacting coastlines with considerable force and causing extensive flooding in coastal areas. As the tsunamis advance, they carry coastal debris, which can collide with structures and inflict substantial damage. Factors such as flow velocity, debris collision, and scour cumulatively affect structures in the tsunami's path (Charvet et al., 2015). Consequently, isolating the damage caused by drifting objects during post-tsunami assessments is challenging. While studies have shown that debris collision can result in structural damage and elevate the risk of building collapse, these collision forces have not been extensively incorporated into structural design considerations (Naito et al., 2014). Moreover, a numerical analysis by Ma et al. (2021) that modeled typical wooden buildings in coastal areas found that including remnants of collapsed structures in their simulations led to a remarkable 150% increase in building failures due to tsunami forces.

Charvet et al. (2015) conducted a vulnerability analysis, concluding that the impact force exerted by floating objects during a tsunami is a crucial determinant of structural collapse risk. Similarly, Palermo et al. (2013) conducted a field investigation of the 2010 Chile Tsunami, finding that impact forces generated by large drifting objects could devastate most structures, especially critical load-bearing components like columns. In the 2011 Tohoku Tsunami, numerous structures succumbed to collision damage from floating debris, including drifting objects (Naito et al., 2014). Furthermore, instances of collision damage involving drifting objects such as storage tanks, trucks, and ships was documented during the 2018 Sunda Strait Tsunami (Stolle et al., 2020).

To understand secondary disaster aspects of tsunamis, such as the collision risks posed by drifting objects, it's essential to first study the behavior of these objects in fluid motion. In this context, Kim et al. (2023) utilized an OpenCV library-based red-green-blue (RGB) analysis approach to track the position of a drifting container affected by a solitary wave cresting over a revetment. This method remains

Received 3 August 2023, revised 13 August 2023, accepted 23 August 2023
Corresponding author Jae Cheol Lee: +82-33-250-6232, essentialee@kangwon.ac.kr

effective even when the drifting objects are overturned as long as the RGB values for the object's side or bottom fall within a predefined range. However, the approach has limitations: it can only track the center of a recognized object, making it less effective at monitoring spinning objects or tracking multiple drifting objects simultaneously.

To overcome these limitations, this study employs the motion analysis program digital image post-processing motion (DIPP-Motion) to track the position of a drifting container affected by solitary waves. We used images from a laboratory experiment conducted by Kim et al. (2023) for this purpose. Five markers were placed on the container: one at each of its four corners and one at the top center. The positions of the drifting objects were then tracked, considering the scale of the solitary wave and the object's weight. This method also allowed for a detailed examination of object behaviors, such as rotation.

2. Method

2.1 Laboratory Experiment

Kim et al. (2023) captured images of containers in motion within a two-dimensional wave tank measuring 37 m in length, 0.6 m in width, 1 m in height, and a water depth (h) of 47 cm. In this experiment, a freeboard (F_b) with a surface height of 5 cm and a total height of 52 cm —constructed from waterproof plywood—is positioned 27.05 m away from the wave paddle, as depicted in Fig. 1. The average roughness of the painted revetment's vertical walls and the land area floor is 0.56 mm. As detailed in Table 1, 1/40-scale container models situated 10 cm from the vertical wall are categorized into two types: half-full (Model-A; $W_{total} = W_0 + W_{\max}/2$) and full models (Model-B; $W_{total} = W_0 + W_{\max}$). These acrylic container models were fabricated according to International Organization for Standardization (ISO) specifications. Table 2 outlines the experimental conditions related to solitary wave heights (A) employed by Kim et al. (2023).

Two cameras were mounted on the revetment to capture a 310-cm section. The images were taken at approximately 0.0167 s intervals, equating to 60 frames per second (fps). Grids were marked on the revetment at 10 cm intervals for drift distance measurement and camera calibration, as shown in Fig. 2.

2.2 DIPP-Motion

In this study, DIPP-Motion (DITECT, 2023), a motion analysis program, was used to assess the drifting behavior of containers affected by solitary waves. The program tracks specified markers by converting the analysis region into grayscale. Using a 10 cm × 10 cm grid scale projected onto the floor of the land area, the distance per pixel can be estimated. Subsequently, a total of five markers are set: one at the center point on the container's upper surface and one at each of its four corners. The program then tracks the container as it drifts due to the solitary wave, as shown in Fig. 2. Velocity and acceleration

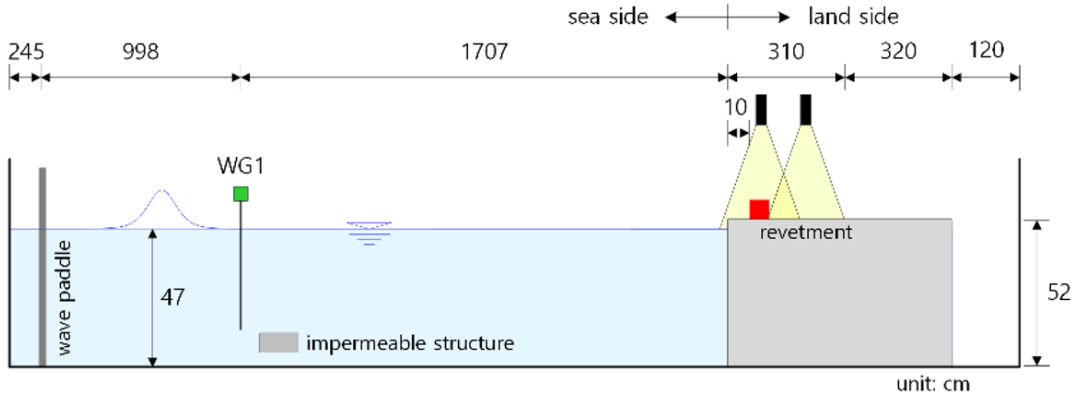

Fig. 1 Conceptual diagram of the wave flume used in the laboratory experiment by Kim et al. (2023).

Table 1 Specifications of a 20 ft container based on ISO standard

20 ft container	Length (mm)	Width (mm)	Height (mm)	Weight W_0 (kg)	Maximum cargo $W_{\max}$ (kg)	Maximum weight W_{total} (kg)
Prototype	6,058	2,438	2,591	2,250	28,230	30,480
Model-A	151	61	65	0.035	0.441	0.256
Model-B						0.476

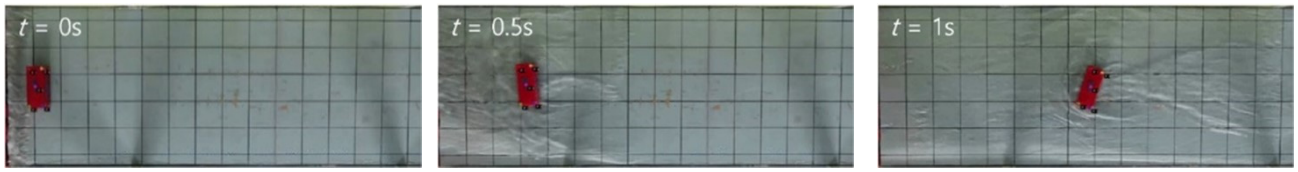

Fig. 2 Tracking process of markers set on the drifting container.

Table 2 Incident wave conditions used in the laboratory experiment

Run	A (cm)	ϵ (A/h)	A/F_b
1	4.4	0.09	0.88
2	5.4	0.12	1.08
3	6.3	0.13	1.26
4	7.2	0.15	1.44
5	8.2	0.18	1.64
6	10	0.21	2
7	12.3	0.26	2.46
8	14.5	0.31	2.9
9	16.5	0.35	3.3
10	18.7	0.4	3.74
11	21.5	0.46	4.3

are calculated based on the markers' initial location and subsequent positions in each frame, factoring in the time interval between the captured image frames.

3. Results

3.1 Effect of Solitary Wave Scale

The scale of the solitary wave is represented by its height. Fig. 3 compares the drift behavior under two different incident solitary wave conditions, specifically $\epsilon = 0.13$ and $\epsilon = 0.18$. Fig. 4 illustrates the spatial distribution of the moving trajectory and velocity of the drifting container under these solitary wave conditions. In Fig. 3, the container model's initial point of drift (t_0) is the reference for the dimensionless time variable, $t^* = (t - t_0)\sqrt{g/h}$, where g is the gravitational acceleration. In Fig. 4, the horizontal distances x and y, as well as the container's moving velocity (V), are non-dimensionalized by dividing them by the sea depth (h) and the solitary wave velocity ($\sqrt{g/h}$), respectively.

The data presented in Fig. 3 demonstrate that the container's moving velocity is higher at $\epsilon = 0.18$ than at $\epsilon = 0.13$, and the drift distance over the same period is also greater when the solitary wave scale is high. According to Lee et al. (2022a), a larger solitary wave scale leads to increased rates of overtopping, and as per Lee et al. (2022b), this results in greater inundation depths in the land area. Consequently, the buoyant force acting on the container increases, reducing floor friction. Furthermore, Fig. 4 reveals that at $\epsilon = 0.18$, the initial acceleration of the drifting container is substantial, the acceleration phase is extended, and the maximum drifting velocity also increases.

Fig. 5 shows the container's maximum drifting velocity (V_{max}) and maximum drifting distance (d_{max}) in dimensionless terms, normalized by the wave speed ($\sqrt{g/h}$) and sea depth (h), respectively. Herein, d_{max} is omitted when it cannot be measured, as it falls outside the 6.3

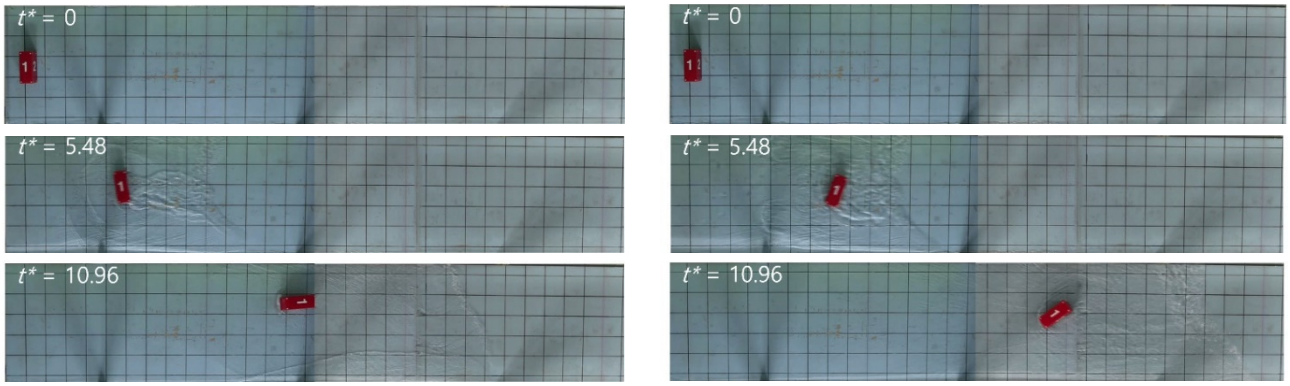

Fig. 3 Container's drifting behavior by solitary wave at $\epsilon = 0.13$ (left) and $\epsilon = 0.18$ (right)

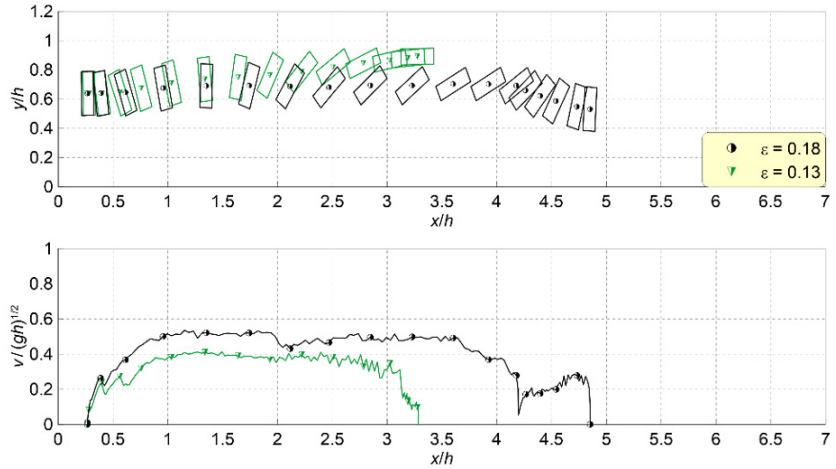

Fig. 4 Spatial distributions of the trajectory (top) and moving velocity (bottom) of the drifting container according to ϵ

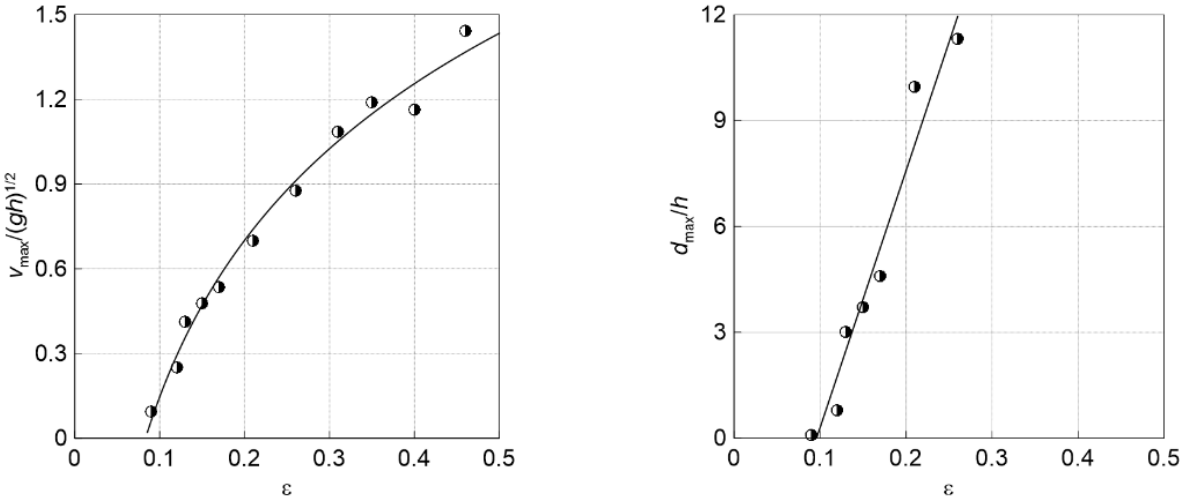

Fig. 5 Maximum drifting velocity (left) and maximum drifting distance (right) of Model-A according to ϵ

m-high land area.

The ratio $V_{\max}/\sqrt{gh}$ increases sharply with the size of the solitary wave. After this rapid increase, the rate of increment starts to taper off. Similarly, $d_{\max}/h$ rises with ϵ. However, a clear trend could not be determined since measurements were not captured for all four incident solitary wave conditions.

3.2 Effect of Container Weigt

Fig. 6 shows the drifting behavior of the container, emphasizing the influence of cargo weight under the solitary wave condition characterized of $\epsilon = 0.18$. Meanwhile, Fig. 7 depicts the movement trajectory and velocity. Models A and B possess weights (W_{total}) of $W_0 + W_{\max}/2$ and $W_0 + W_{\max}$, respectively. Here, W represents the

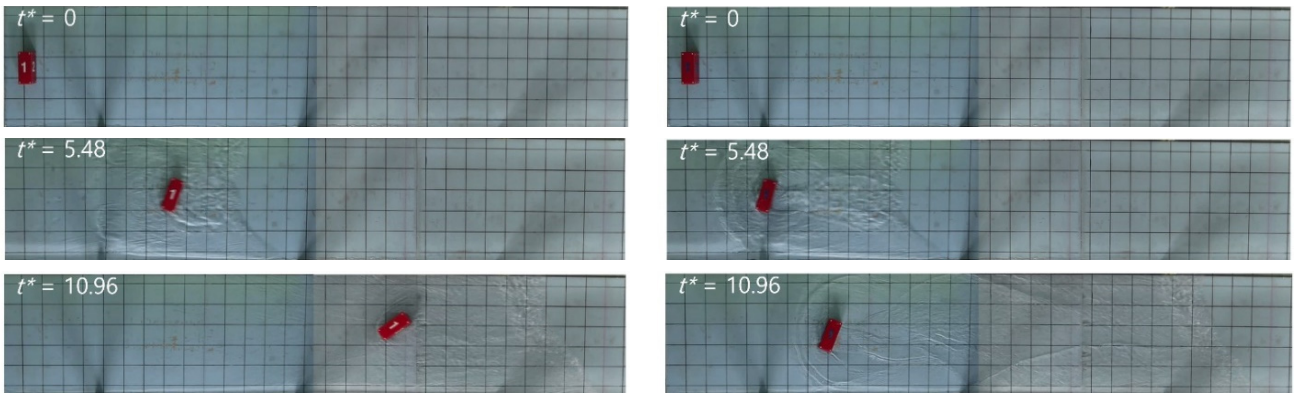

Fig. 6 Drifting behaviors of Container Model-A (left) and Model-B (right) by solitary wave

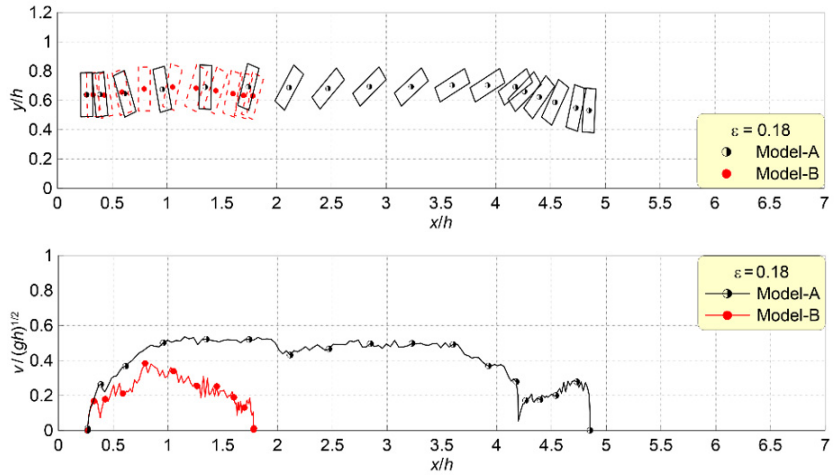

Fig. 7 Spatial distributions of the trajectory (top) and moving velocity (bottom) by solitary wave

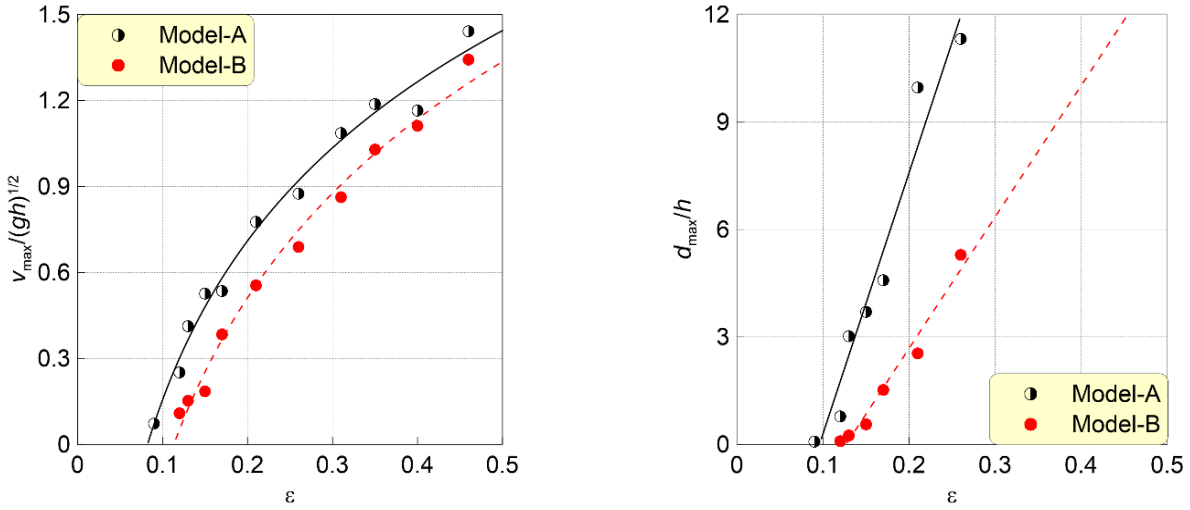

Fig. 8 Distribution of the maximum drifting velocity (left) and maximum drifting distance (right) of the drifting container according to ϵ: comparison according to container weight

combined weight of the empty container and the maximum loaded cargo.

As suggested in Figs. 6 and 7, the difference in the location of the drifting containers, Model-A and Model-B, increases over time under the influence of the solitary wave. Model-B, despite its heavier weight, exhibits lower initial acceleration, moving velocity, and drifting distance compared to Model-A. In the same solitary wave scenario, the buoyant force acts differently based on the container model's weight, leading to this observed trend. Specifically, Model-A, being relatively lighter, experiences better buoyancy at the same depth of immersion, which in turn reduces floor friction. As a result, when comparing $V_{\max}/\sqrt{gh}$ and $d_{\max}/h$ of the drifting container as influenced by the solitary wave based on container weight in Fig. 8, both $V_{\max}/\sqrt{gh}$ and $d_{\max}/h$ generally show less dispersion for Model-A due to its lighter weight.

4. Discussion

In this study, the drifting characteristics of containers influenced by solitary waves, as determined through DIPP-Motion, closely align with the findings of Kim et al. (2023), who utilized an OpenCV library-based RGB analysis technique. Nevertheless, the present investigation allowed for discernment of the container's rotation during drifting and pinpointing the final stationary position of the container—observations that were elusive in the study by Kim et al. (2023). Additionally, despite the experiment's two-dimensional cross-sectional nature, the container exhibited a deviation angle relative to the y-direction center. This might be attributed to inconsistent floor friction or the possibility that the solitary wave did not apply a uniformly distributed load on the container. A positioning technology that can integrate real-time geometric information of drifting objects is essential to fully understand and capture this behavior.

When drifting objects become overturned, DIPP-Motion's location tracking struggles to detect predefined markers. However, our approach has an advantage in that it can concurrently monitor the positions of multiple drifting objects, given its capability to handle several markers simultaneously.

5. Conclusions

This study seeks to explore the drifting behavior of containers influenced by solitary waves, utilizing DIPP-Motion as the motion analysis tool. The overarching aim is to understand tsunamis' secondary disaster characteristics better, focusing on collisions involving drifting objects. Through DIPP-Motion analysis, we examined how the behavior of drifting containers varies with the solitary wave's scale and the container's weight.

As the solitary wave scale grows, both the traveling velocity of the wave and the displacement of the drifting container see a corresponding increase. This behavior can be attributed to larger solitary wave heights resulting in increased immersion depths. This increased depth subsequently diminishes bottom friction and amplifies buoyancy effects. Furthermore, the research indicates that lighter containers, while maintaining a consistent submerged depth, drift at faster velocities and traverse greater distances compared to their heavier counterparts, largely owing to decreased floor friction.

The analytical results related to the drifting behavior of containers propelled by solitary waves emphasize that the scope of secondary disaster damage from collisions is likely to increase with larger tsunami or storm surge scales. Lighter drifting objects are prone to higher velocities, which could affect collision dynamics. However, objects with lower weights generally exert weaker collision forces. As a result, the findings from this study alone make it difficult to precisely quantify the degree of collision damage and to fully understand the complex interplay between the movement velocity and weight of drifting objects.

To further investigate this matter, a follow-up study will conduct hydraulic experiments and computational analyses to examine collision forces. These explorations will focus on determining the relationships between the weight of drifting objects and their collision velocities.

Conflict of Interest

No potential conflicts of interest related to this article were reported.

Funding

This work was supported by the National Research Foundation of Korea (NRF) grant funded by the Korea government (MSIT) (No. 2021R1F1A1062767).

References

Charvet, I., Suppasri, A., Kimura, H., Sugawara, D., & Imamura, F. (2015). A multivariate generalized linear tsunami fragility model for Kesennuma City based on maximum flow depths, velocities and debris impact, with evaluation of predictive accuracy. *Journal of Natural Hazards*, 79(3), 2073−2099.

Digital Image Technology Corporation. (DITECT). (2023). *2D/3D motion analysis software [DIPP-Motion V]*. Digital Image Technology Corporation. https://www.ditect.co.jp/en/software/dipp_motionv.html

Kim, T., Hwang, T., Baek, S., Hong, S., Kim, J., & Lee, W.-D. (2023). Experimental investigations using computer vision for debris motion generated by solitary waves. *Journal of Earthquake and Tsunami*, 291, 108434.

Lee, W. -D., Choi, S., Kim, T., & Yeom, G. -S. (2022a). Comparison of solitary wave overtopping characteristics between vertical and wave absorbing revetments. *Ocean Engineering*, 256, 111542.

Lee, W. -D., Hwang, T., & Kim, T. (2022b). Inundation characteristics of solitary waves according to revetment type. *Water*, 14, 3814.

Ma, X., Zhang, W., Li, X. & Ding, Z. (2021). Evaluating tsunami damage of wood residential buildings in a coastal community considering waterborne debris from buildings. *Engineering Structures*, 244, 112761.

Naito, C., Cercone, C., Riggs, H. R., & Cox, D. (2014). Procedure for site assessment of the potential for tsunami debris impact. *Journal of Waterway Port Coastal and Ocean Engineering, 140, 223−232.*

Palermo, D., Nistor, I., Saatcioglu, M., & Ghobarah, A. (2013). Impact and damage to structures during the 27 February 2010 Chile tsunami. *Canadian Journal of Civil Engineering*, 40(8), 750−758.

Stolle, J., Krautwald, C., Robertson, I., Achiari, I., Mikami, T., Nakamura, R., Takabatake, T., Nishida, Y., Shibayama, T., Esteban, M., Nistor, I., & Goseberg. N. (2020). Engineering lessons from the 28 September 2018 Indonesian tsunami: debris loading. *Canadian Journal of Civil Engineering*, 47(1), 1−12.

Author ORCIDs

Author name	ORCID
Hwang, Taegeon	0000-0002-4959-3906
Kim, Jiwon	0009-0009-4959-4827
Lee, Dong-Ha	0000-0002-6934-1247
Lee, Jae-Cheol	0000-0002-0242-4961